Comparison of the characteristics of atmospheric pressure plasma jets using different working gases and applications to plasma-cancer cell interactions

Hea Min Joh, Sun Ja Kim, T. H. Chung, and S. H. Leem

Citation: AIP Advances **3**, 092128 (2013); doi: 10.1063/1.4823484
View online: http://dx.doi.org/10.1063/1.4823484
View Table of Contents: http://aipadvances.aip.org/resource/1/AAIDBI/v3/i9
Published by the AIP Publishing LLC.

Comparison of the characteristics of atmospheric pressure plasma jets using different working gases and applications to plasma-cancer cell interactions

Hea Min Joh,[1] Sun Ja Kim,[1] T. H. Chung,[1,a] and S. H. Leem[2]
[1]*Department of Physics, Dong-A University, Busan 604-714, Republic of Korea*
[2]*Department of Biological Science, Dong-A University, Busan 604-714, Republic of Korea*

(Received 19 June 2013; accepted 13 September 2013; published online 20 September 2013)

Atmospheric pressure plasma jets employing nitrogen, helium, or argon gases driven by low-frequency (several tens of kilohertz) ac voltage and pulsed dc voltage were fabricated and characterized. The changes in discharge current, optical emission intensities from reactive radicals, gas temperature, and plume length of plasma jets with the control parameters were measured and compared. The control parameters include applied voltage, working gas, and gas flow rate. As an application to plasma-cancer cell interactions, the effects of atmospheric pressure plasma jet on the morphology and intracellular reactive oxygen species (ROS) level of human lung adenocarcinoma cell (A549) and human bladder cancer cell (EJ) were explored. The experimental results show that the plasma can effectively control the intracellular concentrations of ROS. Although there exist slight differences in the production of ROS, helium, argon, or nitrogen plasma jets are found to be useful in enhancing the intracellular ROS concentrations in cancer cells. [http://dx.doi.org/10.1063/1.4823484]

I. INTRODUCTION

Non-equilibrium atmospheric pressure plasma jets (APPJs) are of intense interest in current low-temperature plasma research because of their immense potential for material processing and biomedical applications.[1] The plasma jets generate plasma plumes in open space while providing a significant number of active species, such as radicals, electrons, and ions. Thus, they can be used for direct treatment of materials or living tissues.[2] One of the prerequisites to the biomedical applications is that the plume should be near room temperature and carry a low current under moderate voltage. The use of atmospheric-pressure plasmas in cancer therapies is drawing attentions since plasmas contain short-lived free radicals including reactive oxygen species (ROS), charged species, and electric fields that can induce apoptosis in tumor cells.[3–11] Particularly, APPJs can be utilized in vivo by delivering a lethal dose of plasma to a tumor without harming surrounding healthy tissues.[3,7]

Depending on the jet configuration and the electrical excitation,[2,12–14] the plasma characteristics including heat, charged particle, electric field, and chemically active species may differ significantly.[15] Another important parameter is the kind of utilized working gas (and gas flow rate). Physically, the breakdown mechanism of APPJs depends strongly on the electron multiplication, which controls the transition from Townsend breakdown to streamer breakdown.[16,17] Since the Townsend ionization coefficient and the mobility of charged species in the electric field depend on the gas properties, the gas type determines the electron multiplication and the breakdown mechanism as well as the discharge mode. In addition, different working gases produce different plasma species resulting in different interactions with the targets. Helium, argon, and nitrogen gases have been

[a]Corresponding author: T.H. Chung (thchung@dau.ac.kr)

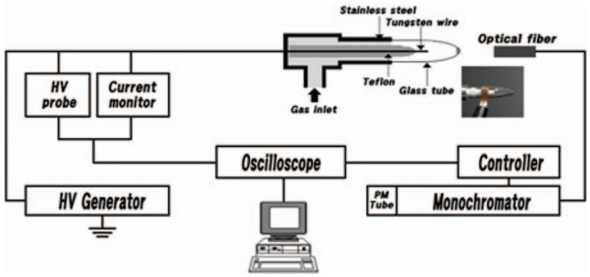

FIG. 1. Schematic of the experimental setup with the diagnostics systems.

mainly utilized in APPJs. For helium, electron multiplication can be easily kept at a low level and glow discharge can be sustained well. For argon, the Townsend's first ionization coefficient is larger and increases faster with the electric field than that for He though much less than that for N_2. The Ar glow discharge can be kept in a small range of the applied field. Electron multiplication in N_2 is very sensitive to the applied field and the transition between Townsend and streamer (filamentary) breakdown occurs suddenly around a certain level of the applied field. The range of the applied voltage for a stable N_2 glow regime is very small.[16] In this paper, a pencil-type plasma jet driven by a low-frequency (several tens of kilohertz) ac and pulsed dc voltages is reported. The gas temperature, the plume length and the optical spectra are measured and compared as functions of the applied voltage, the working gases, and the excitation methods (ac-driven and pulsed dc-driven).

Various effects of atmospheric plasma on live cells have been demonstrated recently.[3,4,18–21] Of particular interest are the plasma interactions with cancerous cells. It has been shown by several groups that the plasma is able to induce death (the programmed death, apoptosis or the necrotic cell rupture) in a number of cancer cell types.[3–11,18–21] Among these, the induction of apoptosis by plasma treatment has proven an intriguing issue. The ROS produced by plasma are considered to be the key constituents that induce apoptosis. The ROS can penetrate the cells and might induce high levels of DNA damage, resulting in apoptosis.[5] Since the discharge characteristics strongly depend on the gas property, different working gases will invoke different effects on plasma-cell interactions. In this work, a preliminary plasma-cell interaction experiment is performed by using three commonly utilized gases such as helium, argon, and nitrogen, and the effects of the plasma exposure to the human lung adenocarcinoma cells (A549) and human bladder cancer cells (EJ) are presented.

II. EXPERIMENTS

Figure 1 shows a schematic of the plasma jet device. The plasma jet consists of two electrodes, Teflon fitting, glass confinement tube (8 mm inner diameter and 10 mm outer diameter), and pencil-shaped nozzle (2 mm inner diameter at the exit). A tungsten pin wire (0.3 mm diameter) with a sharpened tip was inserted coaxially in a glass tube protruding from the stainless steel holder by 13 mm. The glass tube served as dielectric barrier layer and a pencil-shaped nozzle was attached to the end of the glass tube. The distance between the end of the tip and the end of glass tube was approximately 10 mm. The working gas (nitrogen, helium, or argon) was delivered at a flow rate 1 l/min, controlled by a flow meter (RK1600R Kofloc), into the plasma jet and the plasma plume was formed at the end of tip. In the case of nitrogen, a copper ring of 8 mm in length was used as the ground electrode covering partially the outside of the glass tube for the generation of the plasma plume.

Three different kinds of power supplies can be applied. The pulsed dc power supply (PDS4000 FTLab) delivers microsecond (or several hundreds of nanosecond) voltage pulses of up to 3 kV at repetition rates from 10 kHz to 60 kHz. The sinusoidal voltage source of several tens of kilohertz (HPSI 200 FTLab) is applied to the tungsten wire. The ac power supply for the nitrogen discharge is a commercially available transformer for neon light source operated at 20 kHz. The waveforms of the voltage and the current were measured using a real time digital oscilloscope

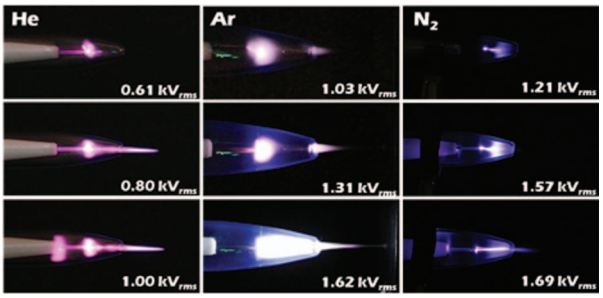

FIG. 2. Photographs of the plasma plumes at different voltages of the 20 kHz sinusoidal ac-driven jets.

(WS44Xs-A LeCroy) via high voltage probe (PPE 20kV LeCroy) and current probe (3972 Pearson). To identify reactive species that are generated in the discharge and subsequently expelled with the gas flow, optical spectra were recorded for emission along the axis of the jet in the range from 200 to 900 nm. The light emitted by the microplasma was focused by means of optical fiber into entrance slit of 0.75 m monochromator (1702, SPEX), equipped with a grating of 1200 grooves per millimeter and slit width of 100 μm. In order to verify the general optical properties of the plasma jets, the optical emissions were measured as a function of time. A photosensor amplifier (Hamamatsu C6386-01) was used to observe the wavelength-integrated plasma emission.

The interaction of the plasma jet with living cells was examined on human lung adenocarcinoma cell lines (A549) and human bladder cancer cell lines (EJ). The cancer cells were propagated in RPMI 1640 (Rosewell Park Memorial Institute; A549) and DMEM (Dulbecco's Modification of Eagle's Medium; EJ) with 10 % fetal bovine serum and 100 U/ml penicillin, respectively. Cells were incubated at 37°C with humidified air and 5% CO_2. A common ROS detection dye, 2′, 7′-dichlorofluorescein diacetate (DCFH-DA) was used to monitor the intracellular ROS production. DCFH-DA passively diffuses into cells. In the presence of ROS, DCFH is rapidly oxidized to highly fluorescent DCF.[22] Fluorescence was measured with excitation and emission wavelengths set at 488 nm and 520 nm, respectively. The cancer cells were pretreated with 10 μM DCF-DA for 5 min at 37% in the dark. The plasma was generated by a sinusoidal ac-driven source. The applied voltage and excitation frequency were 1.15 kVrms and 35 kHz, respectively. The working gas flow rate was kept constant at 100 SCCM (cubic centimeter per minute at STP), unless otherwise stated. Such a reduced gas flow rate is advantageous as it can limit damage by dehydration in sensitive cells and tissue samples. Then, cells were exposed to plasma (and/or gas flow only) for 10 s on nine designated points per dish. Intracellular ROS production was observed in the marked points. The distance from the nozzle to the cell surface was 5 mm. The plasma plume directly reached the cells. After treatment, cells were washed with phosphate buffered saline (PBS). Fluorescence-activated cells were detected using fluorescence microscopy (Nikon TS100-F) and quantified by measuring pixel intensity with Metamorph software (Molecular Devices, Sunnyvale, CA).

III. RESULTS AND DISCUSSIONS

A. Electrical characteristics

The plasma plumes from the 20 kHz sinusoidal voltage-driven jets are shown in Fig. 2 for different working gases (He, Ar, and N_2). In this configuration, the breakdown voltages turn out to be 0.52 kV_{rms} for the helium jet, 0.92 kV_{rms} for the argon jet, and 1.14 kV_{rms} for the nitrogen jets. The plume-out voltages were measured as 0.72 kV_{rms}, 1.0 kV_{rms}, and 1.67 kV_{rms} for the helium, argon, and nitrogen plasma jets, respectively. Since the plasma jets developed in this work employ a sharpened metal tip electrode exposed to the plasma, corona discharge around the metal tip can provide seed electrons to lower the gas breakdown voltage. This allows the plasma jet to be ignited and operated at moderate levels of applied voltage compared to plasma jets utilizing the annular ring electrode.[23] The breakdown voltages were observed to gradually become higher in the order of helium, argon and nitrogen. For nitrogen and argon jets, auxiliary ground electrodes were needed to

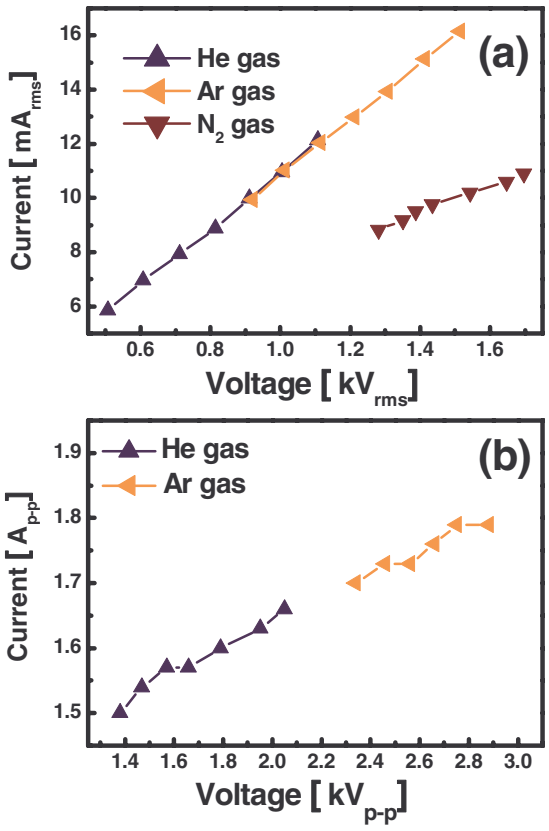

FIG. 3. Total Current as a function of applied voltage with different gases in (a) ac-driven jets at 20 kHz, and (b) pulsed dc-driven jets.

generate plasma plumes in the 1 kV level of the applied voltage. In the nitrogen jet, the copper ring of 8 mm in length was used as the ground electrode. In the argon jet, a planar ground electrode was placed in front of the jet nozzle. The main ionization mechanisms are different depending on the working gas: Penning ionization (for helium), stepwise ionization (for argon), and electron impact ionization (for nitrogen). The ionization rate of helium is the highest among the gases employed in this study. Helium atoms have less excited states than argon atoms and nitrogen molecules. Thus the electrons of helium discharge lose the least energy before the helium atoms are ionized.[24] In the pulsed dc-driven mode operated at a repetition rate of 20 kHz and duty cycles of 10%, the breakdown voltages for the helium and argon jets were 1.34 kV_{p-p} and 2.30 kV_{p-p}, respectively.

Figures 3(a) and 3(b) show the applied voltage and total current curves for the ac-driven jets and the pulsed dc-driven jet, respectively, produced with different working gases at the gas flow rate of 1 L/min. The total current of the pulsed dc voltage-driven jet is found to be generally much larger than that of the sinusoidal voltage-driven jet. The effect of pulsed excitation acts to reduce the amount of power needed to sustain the discharge.

B. Optical characteristics

For a fixed gas flow rate, by increasing the applied voltage, the plasma volume increases, passing through three different stages: the pointed plasma (corona mode), the extended plasma (plasma fills the glass tube) and the plasma jet (plume mode). These developing stages of the plasma are presented along with the temporal evolution of the wavelength-integrated optical emission intensity in Fig. 4. The characteristics of plasma evolvement and light emission differ depending on the working gas type. The different waveforms may result from different discharge mechanisms for corona mode and plasma plume mode. The corona discharge is composed of short-lived pulses at the negative corona

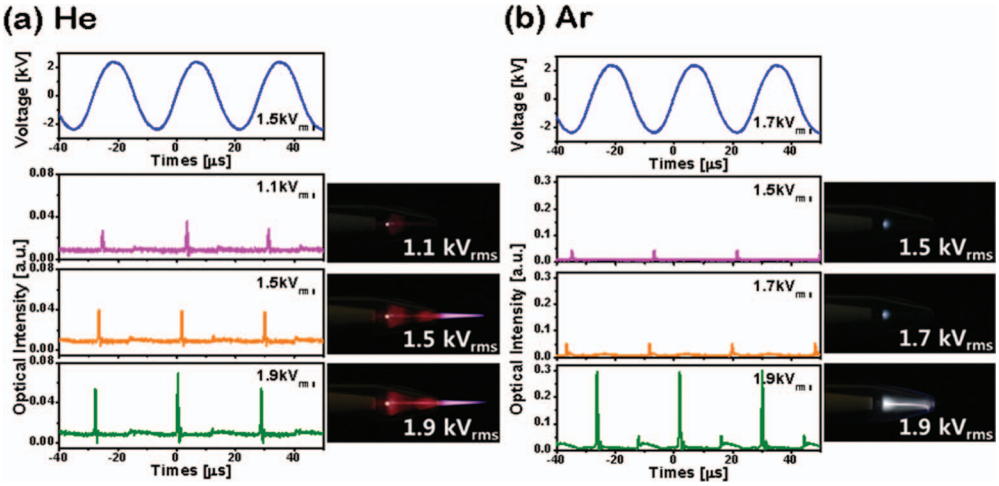

FIG. 4. The developing stages and the temporal evolutions of wavelength-integrated optical intensity of (a) the He and (b) Ar plasma jets.

discharge in needle-plate geometry.[25] With increasing applied voltage, the discharge is found to produce at least one strong plasma bullet in every cycle of the applied voltage.[26] In Ar discharge, the plume mode starts at 1.9 kV_{rms}, and the main optical emission occurs during the rising edge of the positive half cycle of the voltage waveform and the weak light emission signal is found at the falling edge of the positive half cycle. The optical intensity is found to be in phase with the conduction current. However, in corona mode (below 1.8 kV_{rms}), the optical emission occurs in the trough of the applied voltage. At this moment the drifting velocity of the electrons driven away from the electrode is very low when the electrons move to the low field region thus contributing to the formation of point-like discharge electrons (the negative potential electrode tip covered by an electron-cloud). On the other hand, in He discharge the mode transition occurs at much lower voltage (about 1.1 kV_{rms}) because the electron mobility in helium discharge is much larger than that in Ar discharge. Therefore, the He jet does not exhibit the temporal evolution typical to the corona discharge under the parameter range in this study.

Optical spectra were recorded for emission along the axis of the plasma jet in the range from 200 to 900 nm. Figure 5 shows the emission spectra observed in the plasma jet. The different spectra of (a) pulsed dc-driven mode helium (1 L/min, 1.95 kV_{p-p}) (b) pulsed dc-driven mode argon (1 L/min, 2.56 kV_{p-p}), and (c) ac-driven mode nitrogen (1 L/min, 1.54 kV_{rms}) were compared. The discharge produces a significant UV radiation that belongs to transitions of the OH band at 308 and 287 nm, the atomic oxygen lines at 777.4 and 844.6 nm, the N_2 emission bands at 310–440 nm, and the N_2^+ emission bands at 391–428 nm. Helium jet is observed to produce efficiently the ROS. In particular, the OH peak is observed to be very high in argon plasma jet. It was found that the OH emissions were able to last for longer inside the nozzle than both N_2 and Ar emissions.[27] This causes the OH peak to be much higher than other peaks. The Penning ionization of N_2 and the charge transfer to N_2^+ are relatively suppressed in the argon discharge. Xian *et al.* also observed a strong OH emission from Ar plasma jet and much stronger emission intensities of N_2^+ from the helium jet.[28]

The spectrum for the nitrogen plasma jet has a series of NOγ lines. The N_2^+ line is weaker than N_2 second positive system bands, which is quite different from that of the helium jet. The most striking difference is that the nitrogen plasma produces very little emission above 400 nm. In particular, there is little emission at the atomic oxygen lines. The emission spectra from the plasma plumes using various working gases clearly indicate the excited NO, O, OH, N_2, and N_2^+.[2,29–32] Since the critical radicals to cell death are O, NO, and OH radicals, the richness of these species may make the plasma jets suitable for biomedical applications.[33–35]

The excitation temperatures of He or Ar lines were measured by using the Boltzmann plot –method.[36–38] The atomic emission intensity (I_{pq}) of the transition from level p to level q depends

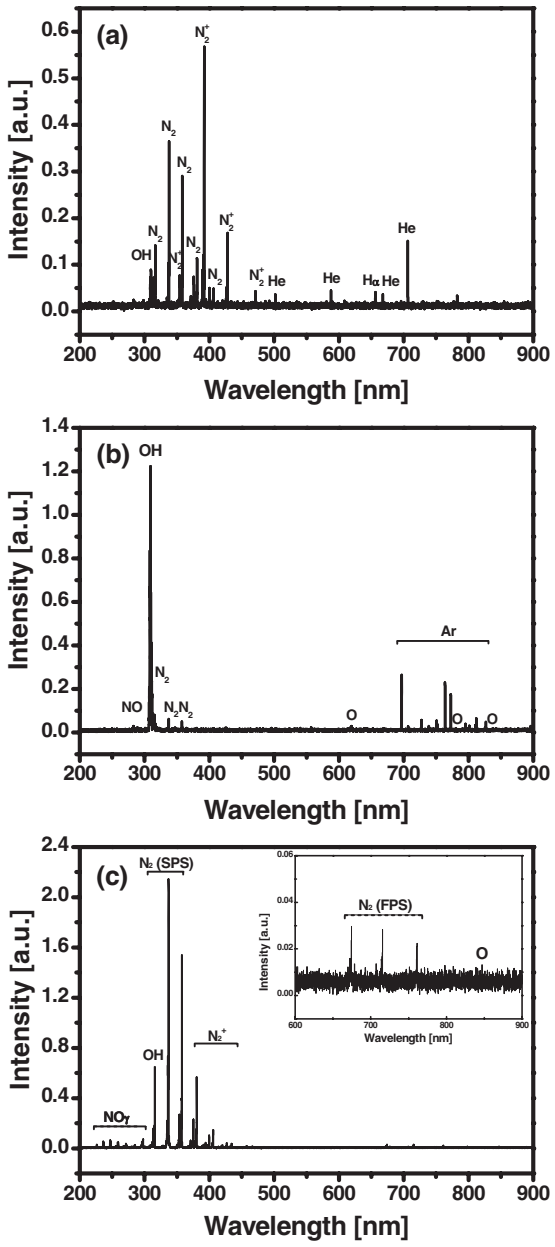

FIG. 5. Emission spectra from 200 nm to 900 nm observed in (a) the pulsed dc-driven helium jet, (b) the pulsed dc-driven argon jet, and (c) the ac-driven nitrogen jet at 20 kHz.

on the transition probability (A_{pq}) and absolute population of the atomic level (n_p), as shown in the following equation; $I_{pq} = n_p A_{pq} h\nu$(where h is the Planck constant and ν is the photon frequency corresponding to the p→q transition). Assuming a Boltzmann distribution of the population of the atomic level, the emission intensity is expressed as $I_{pq} \propto A_{pq} g_p h\nu \exp\left(-\frac{E_p}{k_B T_{exc}}\right)$(where Ep and gp are the energy and degeneracy, respectively, of excited level p, kB is the Boltzmann constant, and Texc is the excitation temperature in Kelvin). From the measurement of intensity and wavelength, a Boltzmann plot is obtained. Using this formula, the electron excitation temperature can be estimated. Figure 6 shows the measurement of Texc in the helium discharge using a set of identified helium atomic lines. In the helium discharge Texc is measured to be 0.15 - 0.16 eV. It is also observed

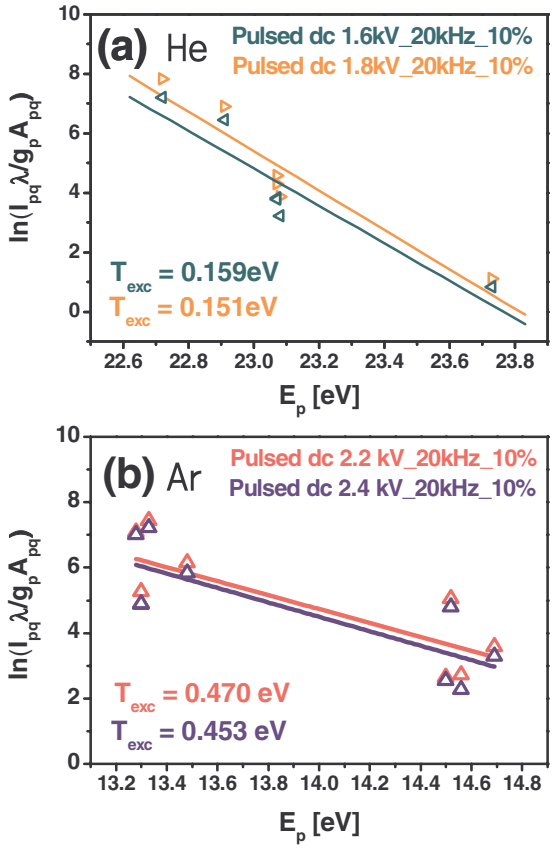

FIG. 6. Boltzmann plot of (a) atomic helium lines and (b) atomic argon lines used to measure Texc in helium and argon discharges.

that the argon discharges have much higher Texc than helium discharges. This indicates that the excitation temperature is determined by the average power.[36]

C. Plume generation

As shown in Fig. 7, the gas temperature and the length of the plasma plume for different gases can be adjusted by the applied voltage. Figure 7(a) shows the measured gas temperature by using a fiber optic temperature sensor (M601-DM&STF, Luxtron). The gas flow rate was kept constant at 1 L/min. The gas temperature remained near room temperature and increased slightly with the applied voltage. As the applied voltage was increased, the length of the plasma plume increased. The plasma plume of helium was observed to be longer than those of other gases, while the Ar plume emitted the strongest light, and the discharge in nitrogen was the weakest.[24]

It is widely accepted that the excitation is due to an ionization wave along the gas channel and is triggered by the kHz excitation inside the source. There are three mechanisms to contribute to the ionization front velocity: electron diffusion, ponderomotive force, and breakdown wave.[39,40] The ionization wave front velocity due to electron diffusion can be expressed as $\upsilon = 2(\nu_i\ D_a)^{1/2}$, where ν_i is the ionization frequency and D_a is the ambipolar diffusion coefficient. For a nonequilibrium plasma, D_a is expressed as $D_a = \mu_+\ kBT_e\ /e$, where μ_+ is the ion mobility and T_e is the electron temperature. Since $\nu_i = \alpha\ \upsilon_d$ (where α is the Townsend's first ionization coefficient and υ_d is the drift velocity of ions), a larger applied voltage results in a larger υ_d, thereby increasing the ionization frequency and ionization wave front velocity. The high bullet velocity is also directly related to the local electric field. Furthermore, the local electric field is proportional to the charges carried by the bullet.[41] When more gas molecules are ionized, a stronger local electric field is induced in front of

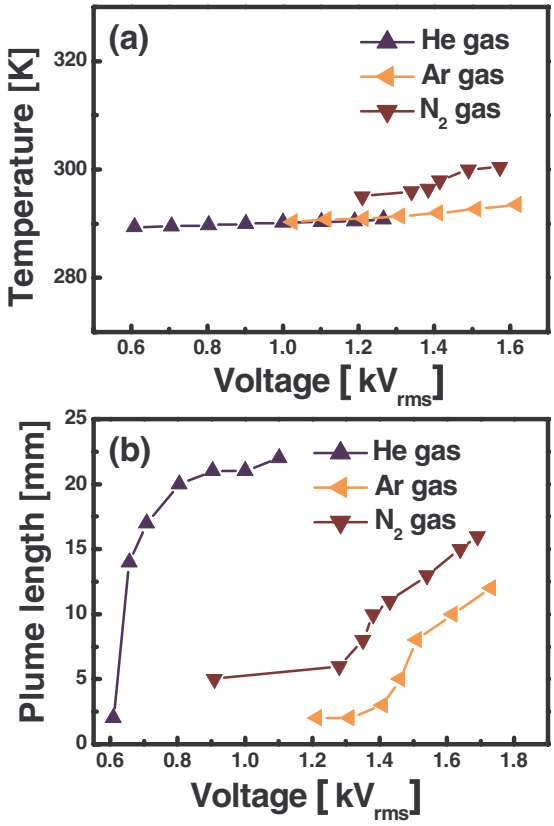

FIG. 7. Comparison of the measured (a) gas temperature and (b) plasma plume length as function of applied voltage for 20 kHz ac-driven jets.

the bullet; in this case, electrons travel toward the bullet head much more quickly, which results in a high bullet velocity. Under a fixed applied voltage, different gases relate to the different velocities of the ionization wave front via α and μ_+. Since $\mu_{+\,He} > \mu_{+\,N2} > \mu_{+\,Ar}$ and $\upsilon_{d\,He} > \upsilon_{d\,N2} > \upsilon_{d\,Ar,}$[42] we have an ordering of $\upsilon_{He} > \upsilon_{N2} > \upsilon_{Ar,}$ because T_e is not much changed in different discharges (although we have a general scaling as $\alpha_{He} > \alpha_{Ar} > \alpha_{N2}$, the effects of μ_+ and υ_d are stronger). This argument is in agreement with the observed plume lengths (L) in the order of $L_{He} > L_{N2} > L_{Ar}$ shown in Fig. 3. In a single pin electrode configuration, the pulsed dc-excited plasma plume was about two times longer than the sinusoidal wave-excited plasma plume.[43]

D. Plasma-cell interaction: Intracellular ROS concentrations

Recent studies have reported that these ROS concentrations were directly related to the mechanism of the death of cancer cells.[6] A certain level of ROS is required for cell survival, while overwhelming ROS can change the equilibrium in cell redox status and lead to damage to proteins, lipids, carbohydrates, and nucleic acids. The first stage of cellular responses to oxidative stress is to use antioxidant defense and repair systems to minimize the damage. However, if the cells are exposed to greater oxidative stress, they can be forced into a permanently growth-arrested state, triggering cell death.[44] The cells tend to vary in their responses to plasma treatment. Cancer cell types have higher metabolic activities than others, and are under increased oxidative stress.[45] This might make them vulnerable to plasma treatment that further augments ROS generation. Figures 8 and 9 show the intracellular ROS fluorescence microscope images of EJ cells and A549 cells, respectively. The results were obtained with different conditions: (8/9a) non-treated control, (8/9b) He gas flow only, (8/9c) the 35 kHz ac-driven He plasma jet at the applied voltage 1.15 kV_{rms}, (8/9d) non-treated control, (8/9e) Ar gas flow only, and (8/9f) the 35 kHz ac-driven Ar plasma jet

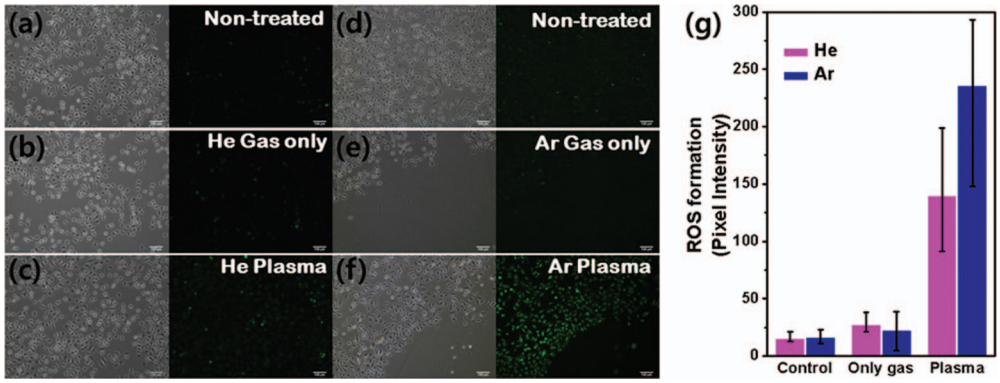

FIG. 8. Intracellular ROS fluorescence microscope images (400×) of different strains after 3 min plasma treatment. The right panels represent the photographs of cells immediately after plasma treatment: (a) non-treated control, (b) He gas flow only, (c) the 35 kHz ac-driven He plasma jet (at 1.15 kV_{rms}), (d) non-treated control, (e) Ar gas flow only, (f) the 35 kHz ac-driven Ar plasma jet (at 1.15 kV_{rms}), and (g) the fluorescence intensities are quantified by measuring pixel intensity with Metamorph software. Each point represents the mean ± SD of three replicates.

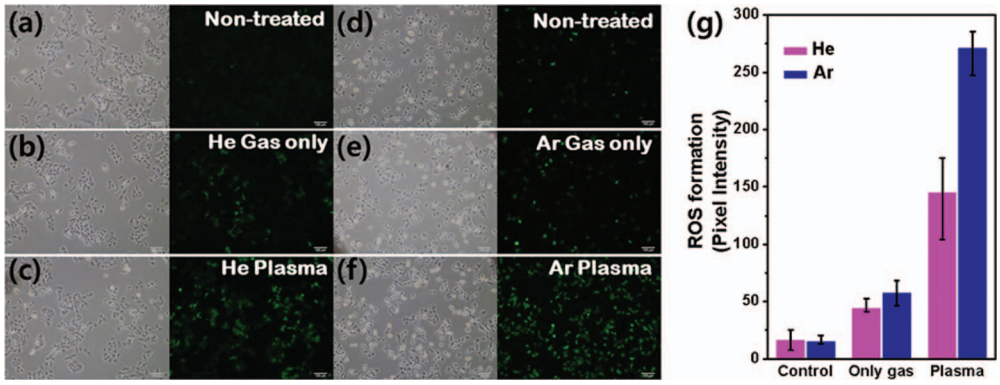

FIG. 9. Intracellular ROS fluorescence microscope images(400×) of different stains after 5 min plasma treatment on A549 cells: (a) non-treated control, (b) He gas flow only, (c) the 35 kHz ac-driven He plasma jet (at 1.15 kV_{rms}), (d) non-treated control, (e) Ar gas flow only, and (f) the 35 kHz ac-driven Ar plasma jet (at 1.15 kV_{rms}), and (g) the fluorescence intensities are quantified by measuring pixel intensity with Metamorph software. Each point represents the mean ± SD of three replicates.

at the applied voltage 1.15 kV_{rms}. In the control (non-treated and gas flow only), a few cells were stained with DCF and the fluorescence intensities were much lower whereas in the plasma-treated cells the fluorescence was increased indicating a high level of DCF staining. Figures 8(g) and 9(g) show the quantification of fluorescence intensity by plasma treatment on the EJ cell and the A549 cell lines. The A549 cells produced higher intracellular ROS concentration than EJ cells.

In our previous study,[46] it was found that the apoptosis rate correlated well with the levels of the intracellular and extracellular ROS. Since the apoptosis rate is directly related to the intracellular ROS level, the Ar plasma may be more effective in the induction of apoptosis for this specific plasma jet configuration. It was observed that intracellular ROS production was dramatically increased in cancer cells by plasma treatment and it could be adjusted by changing the applied condition. Thus, it might provide a promising prospect of cold plasma as a pro-oxidant cancer therapy.

The nitrogen plasma jet has a similar cellular effect to those of He and Ar jets, but needs quite a high breakdown voltage and has a shorter plume length hindering a direct contact with the cell. When a copper ring serves a ground electrode, the generated plasma plume has a longer length up to 8 mm. To confirm the indirect effects of the plasma, the distance from the nozzle to the cell was adjusted. Figure 10 shows the intracellular ROS levels for the direct and indirect plasma treatment on A549 cells. In the case of indirect plasma exposure (Fig. 10(b)), the distance from the nozzle to the cell was 10 mm and the plasma plume reached the media (but did not contact the cells).

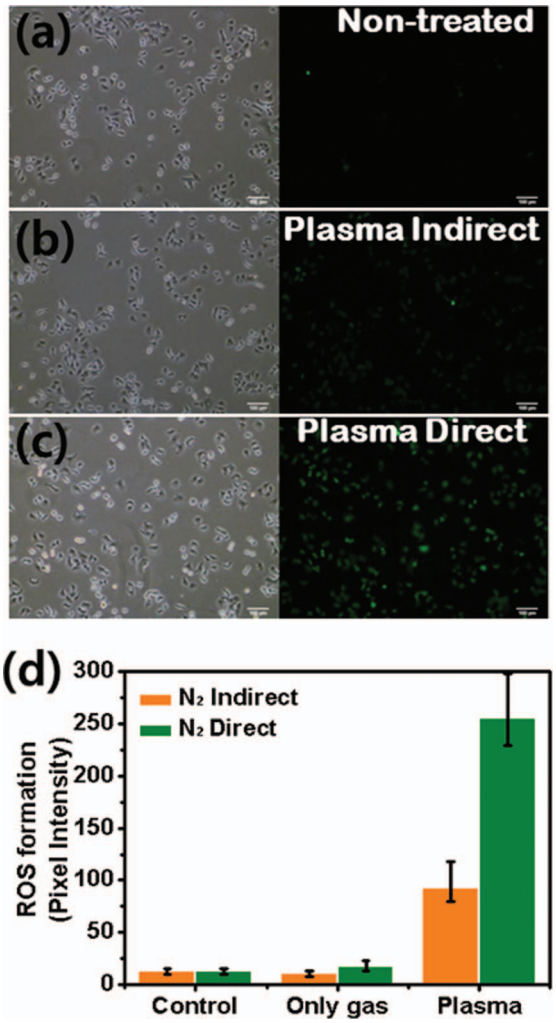

FIG. 10. Fluorescence image of intracellular ROS generation in the nitrogen plasma jet on A549 cells: (a) non-treated control, (b) plasma indirect, (c) plasma direct at 2.12 kV_{rms}, and (d) the fluorescence intensities are quantified by measuring pixel intensity with Metamorph software. Each point represents the mean ± SD of three replicates.

In the case of direct plasma exposure (Fig. 10(c)), the distance from the nozzle to the cell was 5 mm and the plasma plume was in contact with the cells directly. The applied voltage, excitation frequency, and gas flow rate were 2.12 kV_{rms}, 50 kHz, and 0.1 L/min, respectively. As shown in Figs. 10(b) and 10(c), the level of intracellular ROS in the cells exposed to the plasma was increased compared to non-treated control (Fig. 10(a)). Although relatively small, the indirect plasma exposure results in increased ROS concentrations. The direct plasma exposure proved to be more effective in inducing an enhancement of intracellular ROS level. This may be related to the transportability of the plasma species and the penetration to the cells. In this study, it was shown that different cells had different sensitivities to plasma depending on cell types and components of plasma plume in terms of intracellular ROS production.

IV. CONCLUSIONS

APPJs excited at low frequencies utilizing different working gases (helium, argon, or nitrogen gases) were fabricated and characterized. Since different gas properties have different dependences of Townsend ionization coefficient and the mobility of charged species, each discharge demonstrated discharge characteristics unique to the gas type. The emission spectra clearly indicate the excited NO,

O, OH, N_2, and N_2^+ in the plasma plumes generated from these gases. Helium plasmas are observed to be efficient producers of ROS. Especially, the nitrogen plasma jets produced a low concentration of excited oxygen atoms but abundant excited nitrogen species. The breakdown voltages in different working gases gradually become higher in the order of helium, argon, and nitrogen. In a single pin electrode configuration, the plasma plume in the pulsed dc-excited jet was longer than that in the ac-excited jet. The total current of the pulsed dc voltage-driven jet was observed to be much larger than that of the sinusoidal voltage-driven jet. The gas temperature remained near room temperature, which would enable these plasma jets to be adopted for a wide variety of biomedical applications. The potential of plasma jets to induce oxidative stress in EJ cells and A549 cells was evaluated. The experimental results indicate that the A549 cells produce higher intracellular ROS concentration than EJ cells. These observations suggest that different types of human cells differentially respond to the plasma exposure. Although there exist slight differences in the production of ROS, helium, argon, and nitrogen plasmas are found to be useful in enhancing the intracellular ROS concentrations in cancer cells.

ACKNOWLEDGMENT

This work was supported by the National Research Foundation of Korea under Contract No. 2012R1A1A2002591 and 2012R1A1A3010213.

[1] M. Laroussi, M. Kong, G. Morfill, and W. Stolz, *Plasma Medicine* (Cambridge, New York, 2012).
[2] X. P. Lu, Z. Jiang, Q. Xiong, Z. Tang, X. Hu, and Y. Pan, Appl. Phys. Lett. **92**, 081502 (2008).
[3] E. Stoffels, I. E. Kieft, R. E. J. Sladek, L. J. M. van den Bedem, E. P. van der Laan, and M. Steinbuch, Plasma Sources Sci. Technol. **15**, S169 (2006).
[4] G. Fridman, A. Shereshevsky, M. M. Jost, A. D. Brooks, A. Fridman, A. Gutsol, V. Vasilets, and G. Friedman, Plasma Chem. Plasma Process **27**, 163 (2007).
[5] J. Huang, H. Li, W. Chen, G.-H. Lv, X.-Q. Wang, G.-P. Zhang, K. Ostrikov, P.-Y. Wang, and S.-Z. Yang, Appl. Phys. Lett. **99**, 253701 (2011).
[6] X. Yan, Z. Xiong, F. Zou, S. Zhao, X. Lu, G. Yang, G. He, and K. Ostrikov, Plasma Process. Polym. **9**, 59 (2012).
[7] S. Kalghtgi, C. Kelly, E. Cerchar, and J. Azizkhan-Clifford, Plasma Medicine **1**, 249 (2011).
[8] S. J. Kim, T. H. Chung, S. H. Bae, and S. H. Leem, Appl. Phys. Lett. **97**, 023702 (2010).
[9] G. J. Kim, W. Kim, K. T. Kim, and J. K. Lee, Appl. Phys. Lett. **96**, 021502 (2010).
[10] S. Kalghatgi, C. M. Kelly, E. Cerchar, B. Torabi, O. Alekseev, A. Fridman, G. Friedman, and J. Azizkhan-Clifford, PLoS One **6**, e16270 (2011).
[11] J. Y. Kim, Y. Wei, J. Li, P. Foy, T. Hawkins, J. Ballato, and S.-O. Kim, Small **7**, 2291 (2011).
[12] I. E. Kieft, E. P. v. d. Laan, and E. Stoffels, New J. Phys. **6**, 149 (2004).
[13] D. B. Kim, J. K. Rhee, B. Gweon, S. Y. Moon, and W. Choe, Appl. Phys. Lett. **91**, 151502 (2007).
[14] H. S. Park, S. J. Kim, H. M. Joh, T. H. Chung, S. H. Bae, and S. H. Leem, Phys. Plasmas **17**, 033502 (2010).
[15] G. Li, H.-P. Li, L.-Y. Wang, S. Wang, H.-X. Zhao, W.-T. Sun, X.-H. Xing, and C.-Y. Bao, Appl. Phys. Lett. **92**, 221504 (2008).
[16] X. Duan, F. He, and J. Ouyang, Appl. Phys. Lett. **96**, 231502 (2010).
[17] M. Laroussi and T. Akan, Plasma Proc. Polym. **4**, 777 (2007).
[18] A. Shashurin, M. Keidar, S. Bronnikov, R. A. Jurjus, and M. A. Stepp, Appl. Phys. Lett. **93**, 181501 (2008).
[19] A. V. Nastuta, I. Topala, C. Grigoras, V. Pohoata, and G. Popa, J. Phys. D: Appl. Phys. **44**, 105204 (2011).
[20] R. Ma, H. Feng, F. Li, Y. Liang, Q. Zhang, W. Zhu, J. Zhang, K. H. Becker, and J. Fang, Appl. Phys. Lett. **100**, 123701 (2012).
[21] B. Gweon, D. B. Kim, D. Kim, H. Kim, H. Jung, J. H. Shin, and W. Choe, Appl. Phys. Lett. **99**, 063701 (2011).
[22] T. M. Johnson, Z. X. Yu, V. J. Ferrans, R. A. Lowenstein, and T. Rinkel, Proc. Natl. Acad. Sci. **93**, 11848 (1996).
[23] J. L. Walsh and M. G. Kong, Appl. Phys. Lett. **93**, 111501 (2008).
[24] G. Chen, S. Chen, M. Zhou, W. Feng, W. Gu, and S. Yang, Plasma Sources Sci. Technol. **15**, 603 (2006).
[25] X. Li, N. Yuan, P. Jia, and J. Chen, Phys. Plasmas **17**, 093504 (2010).
[26] J. L. Walsh, F. Iza, N. B. Janson, V. J. Law, and M. G. Kong, J. Phys. D: Appl. Phys. **43**, 075201 (2010).
[27] Q. Xiong, A. Y. Nikiforov, X. P. Lu, and C. Leys, J. Phys. D: Appl. Phys. **43**, 415201 (2010).
[28] Y. Xian, X. Lu, Z. Tang, Q. Xiong, W. Gong, D. Liu, Z. Jiang, and Y. Pan, J. Appl. Phys. **107**, 063308 (2010).
[29] X. P. Lu, Z. Jiang, Q. Xiong, Z. Tang, and Y. Pan, Appl. Phys. Lett. **92**, 151504 (2008).
[30] M. H. Guerra-Mutis, Carlos V Pelaez U, and Rafael Cabanzo H., Plasma Sources Sci. Technol. **12**, 165 (2003).
[31] J. L. Walsh, J. J. Shi, and M. G. Kong, Appl. Phys. Lett. **88**, 171501 (2006).
[32] M. Laroussi and X. Lu, Appl. Phys. Lett. **87**, 113902 (2005).
[33] J. F. Kolb, A. A. H. Mohamed, R. O. Price, R. J. Swanson, A. Bowman, R. L. Chiavarini, M. Stacey, and K. H. Schoenbach, Appl. Phys. Lett. **92**, 241501 (2008).
[34] J. Goree, B. Liu, D. Drake, and E. Stoffels, IEEE Trans. Plasma Sci. **34**, 1317 (2006).
[35] Q. Li, X. M. Zhu, J. T. Li, and Y. K. Pu, J. Appl. Phys. **107**, 043304 (2010).

[36] M. Qian, C. Ren, D. Wang, J. Zhang, and G. Wei, J. Appl. Phys. **107**, 063303 (2010).
[37] D. L. Crintea, U. Czarnetzki, S. Iordanova, I. Koleva, and D. Luggenhölscher, J. Phys. D: Appl. Phys. **42**, 045208 (2009).
[38] D. Staack, B. Farouk, A. Gutsol, and A. Fridman, Plasma Sources Sci. Technol. **17**, 025013 (2008).
[39] X. Lu, Q. Xiong, Z. Xiong, J. Hu, F. Zhou, W. Gong, Y. Xian, C. Zou, Z. Tang, Z. Jiang, and Y. Pan, J. Appl. Phys. **105**, 043304 (2009).
[40] J. Shi, F. Zhong, J. Zhang, D. W. Liu, and M. G. Kong, Phys. Plasmas **15**, 013504 (2008).
[41] Q. Xiong, X. Lu, J. Liu, Y. Xian, Z. Xiong, F. Zou, C. Zou, W. Gong, J. Hu, K. Chen, X. Pei, Z. Jiang, and Y. Pan, J. Appl. Phys. **106**, 083302 (2009).
[42] Y. P. Raizer, *Gas Discharge Physics* (Springer, Berlin, 1991).
[43] Q. Xiong, X. P. Lu, K. Ostrikov, Y. Xian, C. Zou, Z. Xiong, and Y. Pan, Phys. Plasmas **17**, 043506 (2010).
[44] H. Pelicano, D. Carney and P. Huang, Drug Resist. Updates. **7**, 97 (2004)
[45] T. Ozben, J. Pharm. Sci. **96**, 2181 (2007).
[46] H. M. Joh, S. J. Kim, T. H. Chung, and S. H. Leem, Appl. Phys. Lett. **101**, 053703 (2012).